FULL PAPER

Dalton
www.rsc.org/dalton

All-iron hydrogenase: synthesis, structure and properties of {2Fe3S}-assemblies related to the di-iron sub-site of the H-cluster †

Mathieu Razavet, Sian C. Davies, David L. Hughes, J. Elaine Barclay, David J. Evans, Shirley A. Fairhurst, Xiaoming Liu and Christopher J. Pickett *

Biological Chemistry Department, John Innes Centre, Norwich, UK NR4 7UH

Received 3rd October 2002, Accepted 3rd December 2002
First published as an Advance Article on the web 21st January 2003

Tripodal dithiolate thioether ligands $MeC(CH_2SH)_2CH_2SR$ (R = Me or Ph) provide a route to {2Fe3S}-complexes and syntheses are described. X-Ray crystal structures for two {2Fe3S}-pentacarbonyl derivatives and that for the first carbonyl cyanide are reported, together with temperature dependent ^{1}H-NMR, Mössbauer, FTIR and redox potential data. The NMR data establish fluctionality associated with inversion at the thioether sulfur in the carbonyl complexes. The Mössbauer data affirm that the coordination environment of the two iron atoms in a dicyanide bridging carbonyl intermediate are differentiated. Bridging carbonyl intermediates have been structurally and spectroscopically identified in resting and CO inhibited forms of the sub-site of all-iron hydrogenases; the observation of a thermally unstable {2Fe3S}-bridging carbonyl intermediate is discussed in this context.

Introduction

The di-iron sub-site of the H-cluster of all-iron hydrogenase catalyses the reduction of protons to dihydrogen at very high rates.[1–6] The sub-site is extraordinary in that: (i) carbon monoxide and cyanide ligands are essential structural elements; (ii) biologically unprecedent Fe^I oxidation states are probably involved in turnover; and (iii) interconversion of bridging and terminal CO ligands may play a key part in the catalysis at the binuclear centre.

X-Ray crystallographic data show that in the oxidised resting state of the H-cluster (H_{ox}) the distal Fe atom of the subsite is ligated by a water molecule or possesses a vacant coordination site, whereas in the carbon monoxide inhibited form, $H_{ox}(CO)$, the site is occupied by CO. It is still unclear whether or not the 2-position of the dithiolate ligand is an NH or CH_2 group. The former is currently preferred on the basis of electron-density arguments and enjoys a conjectural mechanistic role in relaying protons to the distal Fe atom.[3,7,8] A representation of the principle structural features of the sub-site in its paramagnetic resting state is provided by Fig. 1a which is a composite of structural data from two independent crystallographic source codes.[1,2]

How the sub-site of the H-cluster catalyses proton reduction is the subject of extensive spectroscopic and mechanistic studies of the enzyme,[6,9–11] of synthetic assemblies,[12–18] and *in silico* models.[19–22] These are driven in some part by the view that an understanding of the underlying chemistry of the enzyme may inform the design of new electrocatalytic systems for hydrogen production or uptake pertinent to energy transduction technology.

Earlier preparative studies of di-iron assemblies[12–14] have focused on the synthesis of carbonyl cyanide derivatives of the readily accessible {2Fe2S}-core whereas the sub-site is comprised of a {2Fe3S}-core with the three sulfur atoms trigonally capping the iron atom which is proximal to the 4Fe4S-cluster, Fig. 1a. In this paper we describe: (i) the synthesis of the first synthetic {2Fe3S}-carbonyl and carbonyl cyanide compounds and the preparation of the ligands which allow their assembly; (ii) X-ray crystallographic stuctural data for three of the di-iron molecules, including that for the first {2Fe3S}-carbonyl cyanide; and (iii) spectroscopic, dynamic and redox properties of the assemblies, including ^{57}Fe Mössbauer spectra pertinent to differential coordination at the di-iron centres. Some aspects of this work have been described in earlier communications.[18,23,24] The detailed mechanism of cyanation of the {2Fe3S}-core has been the subject of a recent paper.[25]

Results and discussion

Ligand syntheses

The reactions of the tripodal ligand $H_3CC(CH_2SH)_3$ **1** with $[Fe_3(CO)_{12}]$ were first investigated as a route to {2Fe3S}-assemblies, following procedures which are known to give {2Fe2S}-carbonyls with dithiols.[26] The trithiol **1** was prepared as described by Kolomyjec *et al.*[27] However, it was found that **1** reacts with $[Fe_3(CO)_{12}]$ to give intractable black materials. We

† Electronic supplementary information (ESI) available: crystal and structure refinement data for complexes **4a**, **4b** and **5a**. See http://www.rsc.org/suppdata/dt/b2/b209690k/

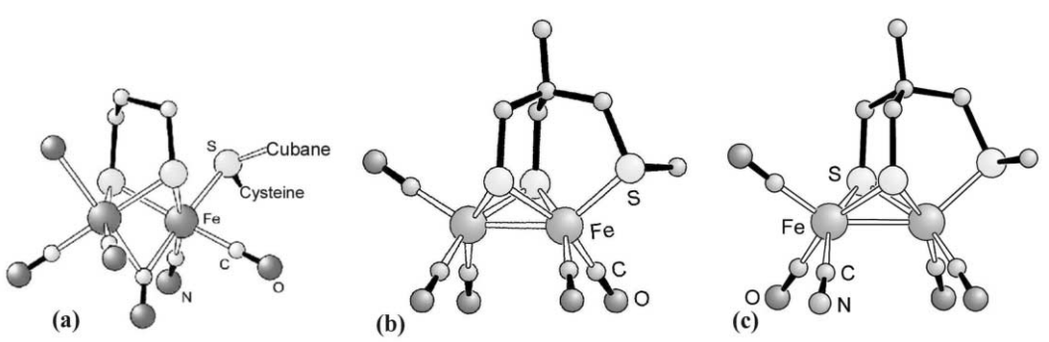

Fig. 1 (a) Proposed structure of the H-cluster of Fe-only hydrogenases; this is a composite model combining features reported by Nicolet *et al.* (PDB code 1HFE)[1] and Peters *et al.* (code 1FEH).[2] (b) Complex **4a**. (c) Monocyanide derivative of complex **5a**.

DOI: 10.1039/b209690k

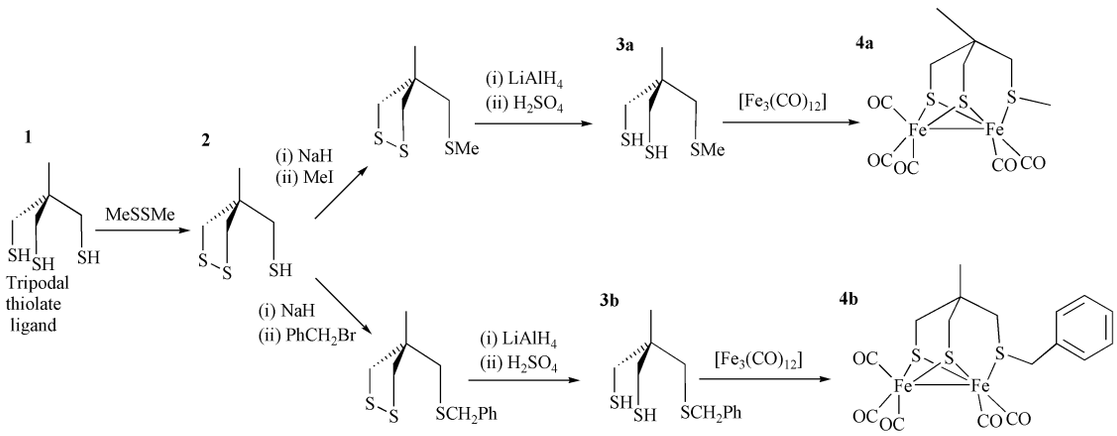

Scheme 1 Synthesis of ligands and complexes **4a** and **4b**.

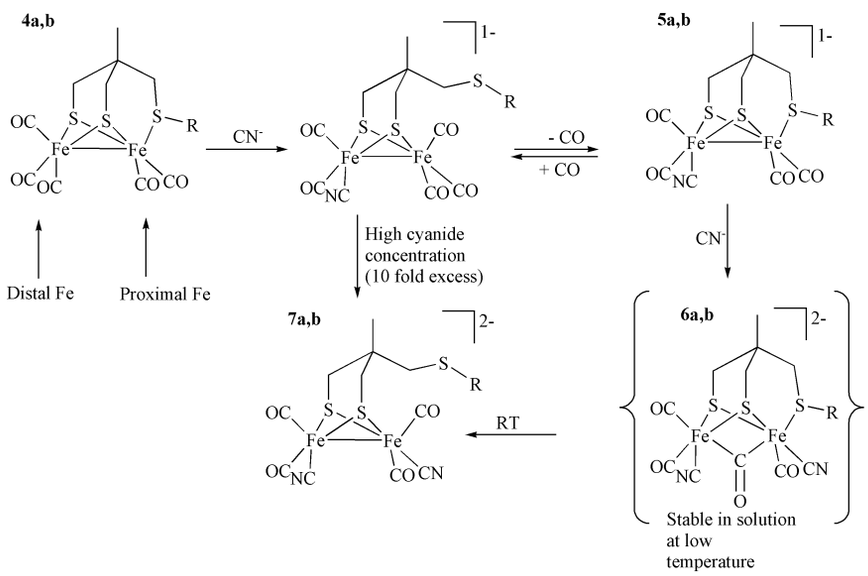

Scheme 2 Synthesis of {2Fe3S}-cyanide assemblies, with R = Me or Bn.

therefore sought to modify the reactivity of **1** by converting it to a dithiolate thioether. This required protecting two of the thiol groups of **1** and leaving the third thiol free for conversion to a thioether. This was achieved by reacting **1** with dimethyldisulfide which leads to oxidative coupling of two of the thiols to give the cyclic disulfide **2** in good yield, Scheme 1. The driving force for the production of **2** is undoubtedly the formation of a stable five membered ring with elimination of volatile methylthiol.

The unprotected thiol group of **2** was deprotonated and reacted with either methyl iodide or benzyl bromide to produce the corresponding thioethers, Scheme 1. Deprotection by reduction of the disulfide bond with $LiAlH_4$ followed by protonation affords the dithiol methyl and benzyl thioethers **3a** and **3b** respectively, Scheme 1.

Synthesis of {2Fe3S}-carbonyls and their cyanide derivatives

The dithiol thioether ligands **3a** and **3b** react with $[Fe_3(CO)_{12}]$ at 90 °C in toluene to afford the complexes $[Fe_2\{MeSCH_2C(Me)(CH_2S)_2\}(CO)_5]$ **4a** and $[Fe_2\{PhCH_2SCH_2C(Me)(CH_2S)_2\}(CO)_5]$ **4b** respectively which were purified by silica gel chromatography, Scheme 1. X-Ray crystallographic analysis of **4a** and **4b** established the formation of the {2Fe3S}-core with differential ligation of the two iron atoms, as discussed more fully below.

The carbonyl complexes **4a** and **4b** react with one equivalent of $[Et_4N][CN]$ to afford the monocyanide salts $[Et_4N][Fe_2\{MeSCH_2C(Me)(CH_2S)_2\}(CN)(CO)_4]$ **5a** and $[Et_4N][Fe_2\{PhCH_2SCH_2C(Me)(CH_2S)_2\}(CN)(CO)_4]$ **5b**. X-ray crystallographic analysis of **5a** shows that the thioether ligand remains coordinated to one iron atom and that the cyanide substitution of CO occurs at the other. Infra-red and Mössbauer data are concordant with **5b** possessing an analogous molecular structure, as described below, Scheme 2.

These deceptively simple stoichiometric substitution reactions mask much interesting chemistry which has been revealed in a recent stopped-flow FTIR mechanistic study.[25] Briefly, the first step involves a fast regioselective attack by cyanide with concerted decoordination of the distal methylthioether ligand. This is followed by a slower re-binding of the thioether with concerted dissociation of carbon monoxide to give the stable {2Fe3S}-monocyanides, Scheme 2.

The FTIR spectral pattern of **5a**,**b** in the CO region is almost identical to that of the unsymmetrical phosphine derivative $[(Me_3P)(CO)_2Fe(SC_3H_6S)Fe(CO)_2(CN)]^-$ isolated by Rauchfuss *et al.*[28] This is expected as both complexes possess similar ligand differentiation at the iron centres. The rather small $+10\ cm^{-1}$ shift in the average ν(CO) for **5a**,**b** *vis a vis* the trimethylphosphine complex attests to the SMe ligand behaving as a remarkably strong electron donor ligand at the Fe^I site.

The reaction of the carbonyl **4a** with two or more equivalents of cyanide proceeds *via* formation of the monocyanide **5a** to give a moderately stable bridging carbonyl dicyanide intermediate **6a** which at room temperature slowly rearranges to the thermally stable all-terminal carbonyl species **7a**, Scheme 2.

The final stable product **7a** has nearly identical spectroscopic properties to those of the {2Fe2S}-dicyanide $[Fe_2(SC_3H_6S)$-

Table 1 Mössbauer parameters (mm s^{-1}) of {2Fe2S}-carbonyl/cyanide and {2Fe3S}-carbonyl/cyanide assemblies at 80 K

	i.s.	q.s.
$[Fe_2(SC_3H_6S)(CO)_6]$ [26,a]	0.04(1)	0.87(1)
	0.03(1)	0.70(2)
$[Fe_2(SCH_2C(CH_2OH)S)(CO)_6]$ [23,a]	0.01(1)	0.95(1)
	0.01(1)	0.75(1)
$[Fe_2\{MeSCH_2C(Me)(CH_2S)_2(CO)_5]$, **4a** [b]	0.03(1)	0.94(1)
	0.12(1)	0.25(1)
$[Fe_2\{PhCH_2SCH_2C(Me)(CH_2S)_2(CO)_5]$, **4b** [c]	0.03(1)	0.98(1)
	0.12(1)	0.27(1)
$[Et_4N][Fe_2\{MeSCH_2C(Me)(CH_2S)_2\}(CN)(CO)_4]$, **5a** [c]	0.05(1)	0.92(3)
	0.11(1)	0.44(3)
$[Et_4N][Fe_2\{PhCH_2SCH_2C(Me)(CH_2S)_2\}(CN)(CO)_4]$, **5b** [a]	0.03(1)	0.78(3)
	0.11(1)	0.39(2)
$[Et_4N]_2[Fe_2(\mu\text{-}CO)\{MeSCH_2C(Me)(CH_2S)_2\}(CN)_2(CO)_3]$, **6a** [c]	0.03(1)	1.13(1)
	0.09(1)	0.68(2)
$[K(18\text{-crown-6})]_2[Fe_2\{MeSCH_2C(Me)(CH_2S)_2\}(CN)_2(CO)_4]$, **7a** [c]	0.03(1)	0.98(1)
$[Et_4N]_2[Fe_2\{PhCH_2SCH_2C(Me)(CH_2S)_2\}(CN)_2(CO)_4]$, **7b** [c]	0.04(1)	1.02(1)
$[Et_4N]_2[Fe_2(SC_3H_6S)(CN)_2(CO)_4]$ [14,c]	0.03(1)	1.09(4)
	0.04(1)	0.86(4)
$[Et_4N]_2[Fe_2(SCH_2C(CH_2OH)S)(CN)_2(CO)_4]$ [14,c]	0.02(1)	1.14(1)
	0.02(1)	0.85(2)

[a] Solid state samples. [b] Frozen acetone solution. [c] Frozen acetonitrile solution.

$(CN)_2(CO)_4]^{2-}$,[12–14] thus the FTIR spectra are superimposable, both complexes show a strong electronic transition at 353 nm, and Mössbauer isomer shift (i.s.) and quadrupole splitting (q.s.) parameters are all very similar, Table 1. This is as expected with the formal remote substitution at the 2-bridgehead position of the 1,3-propane dithiolate having little electronic influence on the di-iron assembly.

Although unstable at room temperature, the intermediate **6a** can be generated from **5a** at low temperature under conditions whereby its isomerisation to **7a** is extremely slow. This has enabled its characterisation by FTIR, UV-visible and Mössbauer spectroscopy. The pertinent spectroscopic observations on **6a** are:

(i) a medium intensity FTIR band at 1780 cm^{-1} which is more than 100 cm^{-1} lower in wavenumber than the group of terminal ν(CO) bands in **6a**;

(ii) the absence of an intense absorption in the 330–380 nm region, observed in the parent material **5a** at 367 nm;

(iii) *two* distinct cyanide bands at 2074 and 2085 cm^{-1}; and

(iv) *two* overlapping ^{57}Fe Mössbauer quadrupole split doublets.

The low energy FTIR band at 1780 cm^{-1}, and its position relative to the terminal bands centred near 1920 cm^{-1}, is characteristic of a bridging carbonyl group. Intense absorption in the 330–380 nm region is characteristic of both {2Fe2S}- and {2Fe3S}-systems possessing metal–metal bonds. Thus observations (i) and (ii) are concordant with the replacement of the Fe–Fe bond by a bridging carbonyl group. Observations (iii) and (iv) establish that the two iron atoms in **6a** have different coordination environments. This spectroscopy and the established stoichiometry of the cyanation reactions, taken together, are fully in accord with the closed-shell dianion **6a** being $[Fe_2(\mu\text{-}CO)\{MeSCH_2C(Me)(CH_2S)_2\}(CN)_2(CO)_3]^{2-}$, Scheme 2. Thioether ligation stabilises the formation of a 'ketonic' bridging carbonyl,[25,29] and accounts for failure to observe bridging carbonyl intermediates in the cyanation reactions of the {2Fe2S}-complex $[Fe_2(SC_3H_6S)(CO)_6]$.

The complex **4b** reacts with cyanide under similar conditions in an analogous fashion giving successively **5b,** the intermediate **6b** and finally **7b**, Scheme 2. From the close similarity of the FTIR spectra of **6b** to that of **6a** together with the rearrangement to **7b**, we infer that **6a** and **b** are structural analogues.

The dianions **6a**,**b** have a particular significance in the context of the di-iron subsite of all-iron hydrogenase which in its CO inhibited form has a {2Fe3S}-core, a bridging CO and two differentiated Fe atoms, each ligated by a single cyanide ligand, Fig. 2.

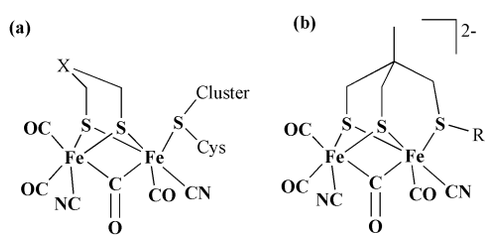

Fig. 2 (a) Proposed structure of H_{ox}–CO, the partially oxidised and CO inhibited form of the sub-site, X = CH_2 or NH and (b) the intermediates **6a**,**b**.

Crystal structure description of {2Fe3S}-assemblies 4a, 4b and 5a

In the crystals of **4a** there are two independent molecules, virtually identical in all aspects, Fig. 1b. The core structures of these molecules are also very similar in shape and size to those of **4b** and **5a**. Molecular dimensions of the four molecules are listed in Table 2, the structure of **4b** is shown in Fig. 3 and that of **5a** in Fig. 1c.

In each complex, both iron atoms are five-coordinate with square pyramidal patterns. The square base in every case comprises two thiolate sulfur atoms, S(1) and S(2), and two carbon

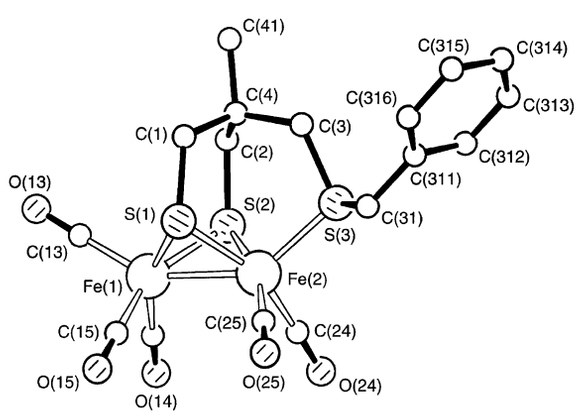

Fig. 3 View of a molecule of **4b**. Hydrogen atoms have been omitted for clarity. In molecules of **4a** and **5a**, C(31) is a terminal methyl group, but their cores are essentially as that of **4b**. O(15) becomes N(15) in the case of **5a**.

Table 2 Selected molecular dimensions in the complexes **4a**, **4b** and **5a**

	4a, mol. A	**4a**, mol. B	**4b**	**5a**
Fe(1) ··· Fe(2)	2.5086(9)	2.5158(10)	2.4969(8)	2.5378(9)
Fe(1)–S(1)	2.2560(12)	2.2537(13)	2.2574(11)	2.2412(12)
Fe(1)–S(2)	2.2549(13)	2.2506(13)	2.2617(11)	2.2486(13)
Fe(1)–C(13)	1.795(5)	1.794(7)	1.779(5)	1.765(4)
Fe(1)–C(14)	1.779(5)	1.787(6)	1.784(5)	1.761(4)
Fe(1)–C(15)	1.795(6)	1.770(6)	1.782(4)	1.941(4)[a]
Fe(2)–S(1)	2.2512(13)	2.2505(14)	2.2516(10)	2.2599(11)
Fe(2)–S(2)	2.2614(12)	2.2563(13)	2.2594(11)	2.2646(14)
Fe(2)–S(3)	2.2508(14)	2.2567(14)	2.2347(10)	2.2547(11)
Fe(2)–C(24)	1.764(5)	1.765(5)	1.764(4)	1.752(4)
Fe(2)–C(25)	1.755(5)	1.772(6)	1.767(4)	1.761(4)
S(2)–Fe(1)–S(1)	85.94(4)	86.34(5)	85.49(4)	86.60(4)
C(13)–Fe(1)–S(1)	103.06(14)	97.06(17)	102.77(15)	99.42(14)
C(14)–Fe(1)–S(1)	156.22(17)	160.7(2)	157.09(17)	160.04(15)
C(15)–Fe(1)–S(1)	86.65(15)	87.73(18)	86.59(15)	87.92(13)
C(13)–Fe(1)–S(2)	102.88(15)	103.60(18)	104.02(15)	104.12(14)
C(14)–Fe(1)–S(2)	86.49(17)	86.81(17)	87.23(15)	88.71(13)
C(15)–Fe(1)–S(2)	157.87(18)	154.7(3)	154.12(14)	158.10(13)
C(14)–Fe(1)–C(13)	100.6(2)	102.1(3)	100.1(2)	100.5(2)
C(15)–Fe(1)–C(13)	99.1(2)	101.5(3)	101.7(2)	97.68(18)
C(14)–Fe(1)–C(15)	92.0(2)	90.8(2)	90.6(2)	89.25(18)
S(1)–Fe(2)–S(2)	85.91(5)	86.28(5)	85.68(4)	85.78(5)
S(3)–Fe(2)–S(1)	96.95(5)	94.63(5)	100.37(4)	94.34(4)
C(24)–Fe(2)–S(1)	162.11(16)	161.31(17)	158.84(13)	162.84(13)
C(25)–Fe(2)–S(1)	87.28(16)	88.16(17)	88.69(13)	88.99(15)
S(3)–Fe(2)–S(2)	96.14(5)	97.08(5)	90.78(4)	98.42(5)
C(24)–Fe(2)–S(2)	89.09(14)	89.87(16)	90.00(15)	90.75(14)
C(25)–Fe(2)–S(2)	160.34(16)	160.45(18)	164.93(13)	159.35(16)
C(24)–Fe(2)–S(3)	100.66(16)	103.99(16)	100.39(13)	102.79(13)
C(25)–Fe(2)–S(3)	102.98(16)	102.05(17)	103.99(13)	101.90(16)
C(25)–Fe(2)–C(24)	91.8(2)	89.4(2)	90.24(19)	88.4(2)
Fe(2)–S(1)–Fe(1)	67.64(4)	67.91(4)	67.25(3)	68.64(4)
Fe(1)–S(2)–Fe(2)	67.49(4)	67.86(4)	67.05(3)	68.43(4)
Displacement (Å) towards apical ligand of iron atoms from square base mean-plane				
Fe(1)	0.392(1)	0.380(1)	0.4171(9)	0.3674(9)
Fe(2)	0.317(1)	0.327(1)	0.3075(9)	0.3231(9)
Angle (°) between normals to square-base mean-planes				
	74.11(5)	75.04(5)	72.49(4)	76.67(4)
Torsion angles (°), C(4)–C(3)–S(3)–C(31)				
	–104.9(4)	–100.8(4)	–134.3(3)	–99.4(3)

[a] Cyanide ligand.

atoms (of carbonyl ligands in every case except in complex **5a** where C(15) is of a cyanide ligand). The Fe(1) iron atoms are displaced *ca.* 0.39 Å from its base plane towards the apical carbonyl ligand, and the Fe(2) atoms *ca.* 0.32 Å towards the thioether S(3) atom. The square planes are hinged sharply through S(1) and S(2) and the two iron atoms can thus form an Fe–Fe bond with length between 2.497(1) Å in **4b** to 2.538(1) Å in **5a**; the angles between the normals to the two base planes range correspondingly from 72.5(1) to 76.7(1)°. The S_3 ligand sits symmetrically about a pseudo-mirror plane above the $Fe_2(CO)_5$ or $Fe_2(CO)_4(CN)$ unit, with the C(31) group projecting out one side or the other from that plane; the C(4)–C(3)–S(3)–C(31) torsion angles are *ca.* −101° in the **4a** and **5a** molecules, and rather larger, −134.3(3)°, in **4b** where C(31) is the methylene carbon of the benzyl group.

The principal variations in dimensions in this series of complexes result from the replacement of the carbonyl ligand C(15)–O(15) by a cyanide ligand in complex **5a**; this replacement also changes the overall charge on the complex, from zero to anionic (−1). The Fe ··· Fe distance is lengthened in this complex, and all other coordination distances about Fe(1) are correspondingly shorter; the dimensions about Fe(2) appear little affected by the substitution.

The structural similarities between the enzyme sub-site and the model compounds are evident from Fig. 1. For example, the Fe ··· Fe bond distance in **5a** and the average bridging Fe–S bond lengths are similar to those distances estimated from the protein crystallographic data, which are 2.6 and 2.3 Å respectively, but the thioether Fe–S distance in **5a** at 2.25 Å is somewhat shorter than the corresponding sub-site Fe–$S_{cysteine}$ distance in the enzyme which is *ca.* 2.5 Å.[1,2]

Solution dynamics of carbonyls 4a and 4b

Rauchfuss and co-workers described a fluctional process for the dithiolate complex $[Fe_2(SC_3H_6S)(CO)_6]$ which is associated with

flipping of the propane backbone.[13] This process is not possible for **4a** or **4b** because the backbone is locked into position by the coordinated thioether group. However, **4a** and **4b** do show dynamic solution processes which are associated with inversion at the thioether sulfur. The evidence for this is as follows.

Variable temperature ^{1}H NMR of **4a** and **4b** in deuterated dichloromethane revealed the presence of a dynamic process, as shown for the methyl derivative by Fig. 4 and for the benzyl derivative by Fig. 5. The static spectra were recorded for the Me and benzyl derivatives at low temperature. Fig. 6 shows the experimental data for **4a** at 233 K together with the spectrum simulated using the program *gNMR*.[30] The dynamic process of **4a** can be represented as a combination of two independent spin systems. Namely, two inter-converting ABCD spin systems

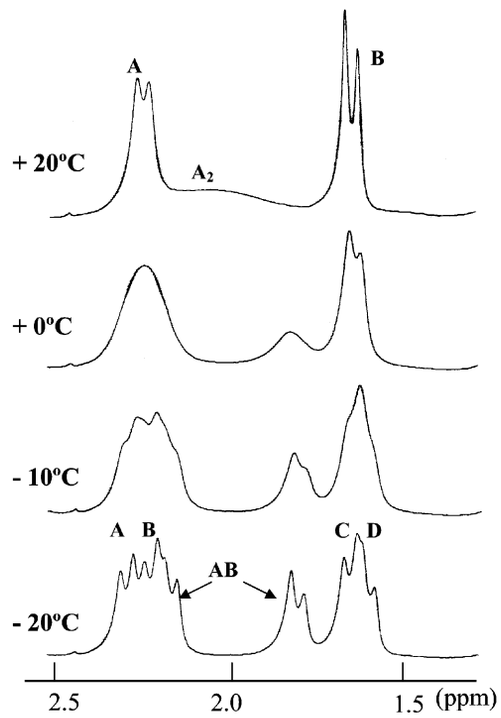

Fig. 4 Variable temperature ^{1}H NMR spectrum of **4a** in CD_2Cl_2 (–SCH_3 protons at 2.62 ppm not shown).

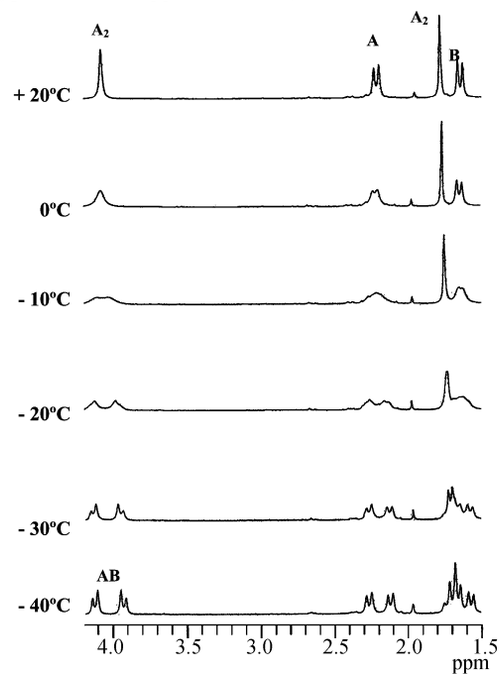

Fig. 5 Variable temperature ^{1}H NMR spectrum of **4b** in CD_2Cl_2. Peak at 1.97 ppm is CH_3CN.

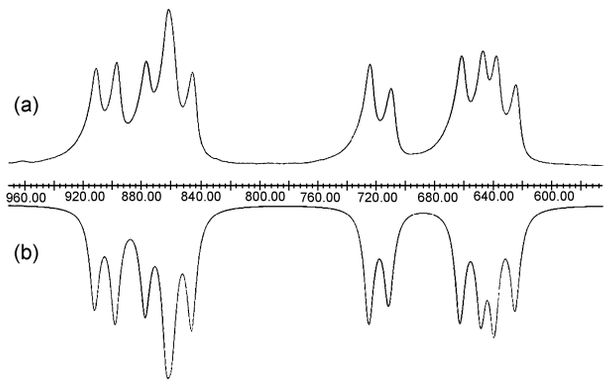

Fig. 6 (a) Experimental and (b) simulated ^{1}H NMR spectra of **4a** at 233 K.

which, as the temperature is raised, coalesce into two identical AB spin systems *i.e.* ½ (ABCD) + ½ (ABCD)′ ⟶ 2AB, plus an isolated AB pair which coalesces to an A_2 spin system, Fig. 4. The energetics of the common AB ⟶ A_2 system for **4a** and **4b** was not analysed because of overlap with the ABCD system. An additional AB ⟶ A_2 system is observed in **4b**, Fig. 5. Chemical shift and integration parameters show that the ABCD system is associated with the methylene groups attached to the bridging sulfur atoms and the isolated AB pair with the methylene group attached to the thioether ligand for both **4a** and **4b**. The additional AB ⟶ A_2 system of **4b**, centred at 4.05 ppm in Fig. 5, is correspondingly associated with the methylene of the S–CH_2Ph group.

The interconverting spins systems are readily explained by inversion at the thioether sulfur as represented in Fig. 7. The second AB ⟶ A_2 system of **4b** must arise from restricted rotation about the SCH_2Ph group leading to inequivalence of the methylene protons when the sulfur inversion is frozen-out.

The activation free energies $\Delta G^{\ddagger}$ for the inversion process of **4a** and **4b** were determined by simulation of spectra over a range of temperature. A typical plot is illustrated by Fig. 8 which shows ln k/T *versus* $1/T$ for **4b** using values of k determined by simulation of the ABCD system. Table 3 summarises the $\Delta G^{\ddagger}$ data obtained by this method. It is evident from this table that the energetics for the inversion of **4a** and **4b** are quite similar with $\Delta G^{\ddagger}$ (and $\Delta H^{\ddagger}$) differing by less than 10 kJ mol^{-1}.

Included in the table are data for the AB ⟶ A_2 spin-system which is associated with restricted rotation around the S–CH_2Ph bond. The magnitude of $\Delta G^{\ddagger}$ is close to that for inversion process of **4b** and this can be explained by the activation free-energy barrier to rotation being larger than that for inversion, *i.e.* rotation is frozen out at a higher temperature than the inversion which is consequently rate limiting. However, $\Delta H^{\ddagger}$ and $\Delta S^{\ddagger}$ components of the free-energy of activation for the two spin systems differ substantially suggesting that the barrier to rotation may be lower or comparable with that for inversion, Table 3.

Solid and solution state Mössbauer parameters

Mössbauer parameters for the {2Fe2S}-carbonyl/cyanide and {2Fe3S}-carbonyl/cyanide complexes are given in Table 1. The isomer shift (i.s.) values of the {2Fe2S}-hexacarbonyl complexes are consistent with those reported earlier for related complexes.[31,32] Previously, we fitted the solid state spectrum of [$Fe_2(SC_3H_6S)(CO)_6$] to one doublet.[14] However, a more rigorous analysis shows a better fit of the spectrum by two, overlapping, quadrupole split doublets with similar i.s. but different q.s.. The origin of the differentiation of the iron sites in the solid state is thought to be the positioning of the propanedithiolate CH_2 above one of the iron atoms. In solution this differentiation is lost, due to the fluctionality of the propanedithiolate unit,[13] and

Table 3 Activation parameters for spin systems obtained from the simulation [30]

	4a, ABCD ⟶ AB	**4b**, ABCD ⟶ AB	**4b** (centred at 4.05 ppm), AB ⟶ A_2
$\Delta H^{\ddagger}$/kJ mol^{-1}	58.8	64.9	82.0
$\Delta S^{\ddagger}$/J K^{-1} mol^{-1}	8.8	47.9	109.5
$\Delta G^{\ddagger}_{298}$/kJ mol^{-1}	56.2	50.6	49.3

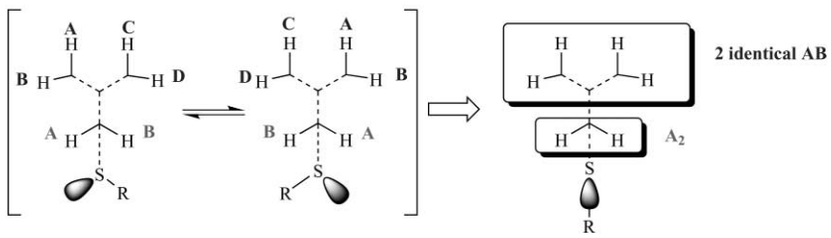

Fig. 7 Schematic representation of the ABCD ⟶ AB and AB ⟶ A_2 systems for both **4a** and **4b** (view from the apical methyl on top of the ligand).

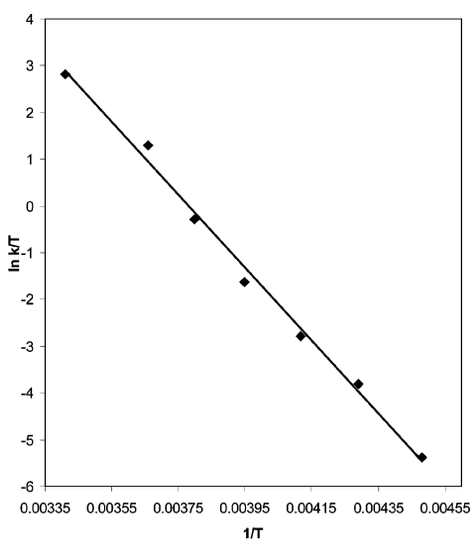

Fig. 8 Eyring plot obtained from estimated values of k, for the ABCD system of **4b**.

a single quadrupole split doublet is hence observed (i.s. = 0.03(1); q.s. = 0.81(1) mm s^{-1}).

The spectra of the {2Fe3S}-pentacarbonyls **4a** and **4b** in frozen acetone solution show two, well defined, overlapping, quadrupole split doublets, Fig. 9; one of the iron atoms is now differentiated from the other by binding of a thioether sulfur. The parameters for *one* of the doublets are similar to those of the $[Fe_2(SC_3H_6S)(CO)_6]$ complexes, those of the other doublet are significantly different, exhibiting a larger i.s. and smaller q.s., and can therefore be assigned to the iron atom ligated by the thioether sulfur. The replacement of a terminal carbonyl group (π-acceptor) by a thioether lowers the s-electron density at the metal, which is reflected by the increase in i.s., and replacement of a π-acceptor by a non-π-acceptor causes a decrease in q.s. There is no significant difference between the parameters obtained for **4b** in frozen solution and in the solid state. The Mössbauer spectrum of **4b** was also recorded at 300 K, the change in i.s. was as expected and the q.s. was shown to be independent of temperature (i.s. = −0.03(1), 0.05(1); q.s. = 1.03(1), 0.31(1) mm s^{-1}).

The mono-cyanide derivatives **5a** and **5b** and the carbonyl bridged, dicyano-derivative **6a** also show two well-defined doublets in frozen solution as observed for **4a** and **4b**. This is fully consistent with thioether sulfur being ligated to one iron atom and the formal oxidation state of the iron atoms remaining iron(I). Importantly, when complex **6a** isomerises to **7a** in which there is no carbonyl bridge and no ligation by thioether sulfur and therefore essentially undifferentiated iron atoms, a single doublet is observed with parameters similar to those of the doublets of $[Fe_2(SC_3H_6S)(CN)_2(CO)_4]^{2-}$ and $[Fe_2(SCH_2C(CH_2OH)S)(CN)_2(CO)_4]^{2-}$, Table 1.

The Mössbauer parameters at 4.2 K for the 2Fe subcluster in iron-only hydrogenase from two organisms have been reported. The reduced 2Fe subcluster from *C. pasteurianum* has an i.s. and a q.s. respectively of 0.08 and 0.87 mm s^{-1}.[10] The oxidised,

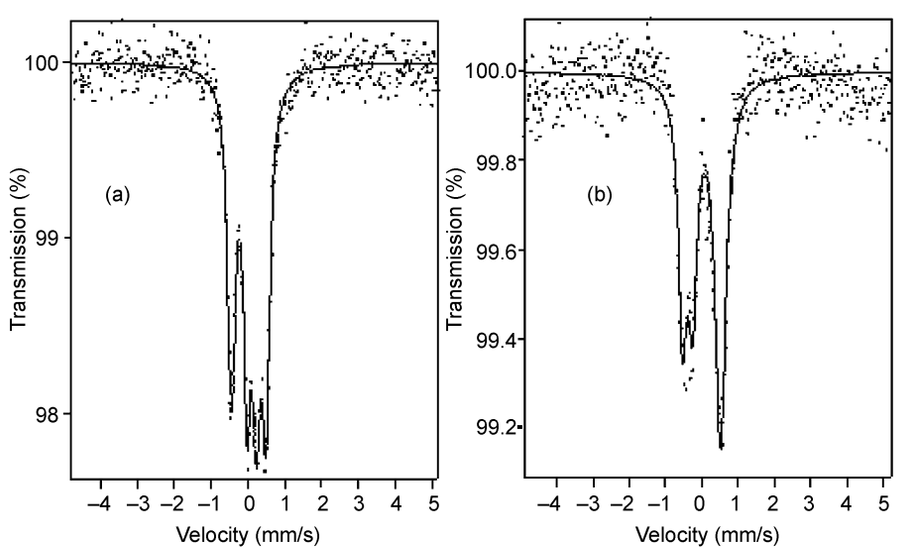

Fig. 9 Selected Mössbauer spectra recorded at 80 K (frozen solution samples). (a) $[Fe_2\{MeSCH_2C(Me)(CH_2S)_2\}(CO)_5]$ (acetone) **4a**, (b) $[Et_4N]_2[Fe_2(\mu\text{-}CO)\{MeSCH_2C(Me)(CH_2S)_2\}(CN)_2(CO)_3]$ (acetonitrile) **6a**.

Table 4 Primary redox potentials of {2Fe3S}-carbonyl/cyanide assemblies referenced against calomel, at 25 °C, in MeCN (0.1 M $[NBu_4][BF_4]$)

Entry	Compound	E_p^{red}/V	E_p^{ox}/V
1	$[Fe_2(SCH_2C(CH_2OH)S)(CO)_6]$ [23]	−1.28	1.3
2	$[Fe_2(SC_3H_6S)(CO)_6]$ [26,35]	−1.32	1.15
3	$[Fe_2\{MeSCH_2C(Me)(CH_2S)_2\}(CO)_5]$, **4a**	−1.38 [b]	0.67
4	$[Fe_2\{PhCH_2SCH_2C(Me)(CH_2S)_2(CO)_5]$, **4b**	−1.36 [b]	0.77
5	$[Fe_2(SC_3H_6S)(CO)_5(PMe_3)]$ [16,c]	−1.97	0.13
6	$[Fe_2\{MeSCH_2C(Me)(CH_2S)_2\}(CN)(CO)_4]^-$, **5a**	−1.83	0.17
7	$[Fe_2\{PhCH_2SCH_2C(Me)(CH_2S)_2\}(CN)(CO)_4]^-$, **5b**	−1.83	0.12
8	$[Fe_2(SC_3H_6S)(CN)(CO)_5]^-$ [16,c]	−1.84	0.46
9	$[Fe_2(SC_3H_6S)(CN)(CO)_4(PMe_3)]^-$ [16,c]	−2.25	−0.06
10	$[Fe_2(\mu\text{-}CO)\{MeSCH_2C(Me)(CH_2S)_2\}(CN)_2(CO)_3]^{2-}$, **6a** [a]	≤ −2.40	−0.10 [b]
11	$[Fe_2\{MeSCH_2C(Me)(CH_2S)_2\}(CN)_2(CO)_4]^{2-}$, **7a**	≤ −2.40	−0.25
12	$[Fe_2\{PhCH_2SCH_2C(Me)(CH_2S)_2\}(CN)_2(CO)_4]^{2-}$, **7b**	≤ −2.40	−0.26
13	$[Fe_2(SCH_2C(CH_2OH)S)(CN)_2(CO)_4]^{2-}$ [14]	−2.36	−0.08
14	$[Fe_2(SC_3H_6S)(CN)_2(CO)_4]^{2-}$ [14,16]	−2.33	−0.11

[a] Recorded at −45 °C. [b] Partially reversible. [c] Corrected to SCE.

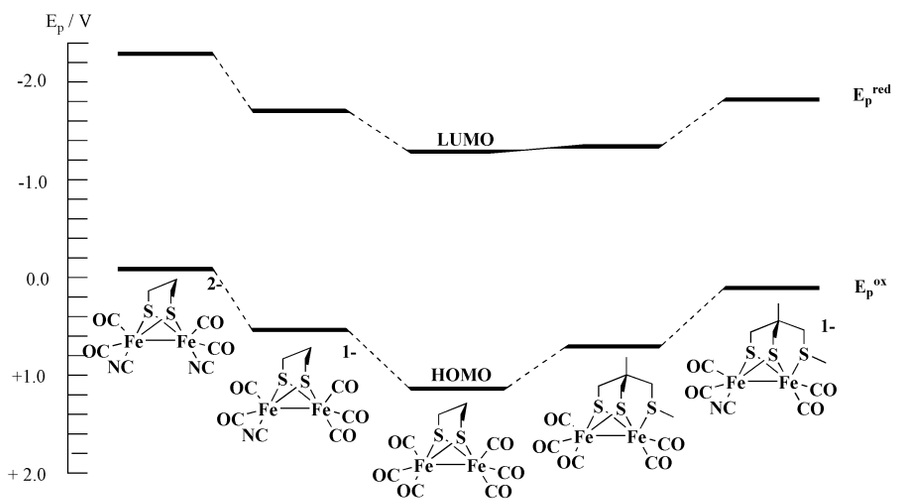

Fig. 10 Evolution of HOMO and LUMO of {2Fe3S}-assemblies as qualitatively measured by solution oxidation and reduction potentials E_p^{ox} and E_p^{red} *versus* SCE respectively.

CO inhibited 2Fe subcluster of *D. vulgaris* has i.s. 0.13 and 0.17, and q.s. 0.65 and 0.70 mm s^{-1}.[11] The i.s. range of 0.11–0.15 mm s^{-1} (adjusted to 77 K ‡) for the 2Fe subcluster of the oxidised, CO inhibited form of the enzyme active site has been compared[11] to the values we have previously reported[14] for {2Fe2S}-assemblies. As the i.s. of the synthetic iron(I)/iron(I) assemblies were smaller than those observed in the enzyme, an iron(II)/iron(III) assignment was favoured (*i.e.* reduced 2Fe subcluster = iron(II)/iron(II); oxidised 2Fe subcluster = iron(II)/iron(III)). However, it is clear from this work that i.s. values from the more closely analogous {2Fe3S}-synthetic assemblies fall well within the range found for the 2Fe subcluster. The Mössbauer parameters of the enzyme 2Fe subcluster do not, therefore, exclude the possibility of an iron(I)/iron(I) (*i.e.* reduced 2Fe subcluster = iron(I)/iron(I); oxidised 2Fe subcluster = iron(I)/iron(II)) system in iron-only hydrogenase.

Primary oxidation and reduction potentials of {2Fe3S}-systems

The primary oxidation and reduction peak potentials, E_p, of the various {2Fe3S}-complexes were measured by cyclic voltammetry in MeCN–0.1M $[NBu_4][BF_4]$ and are given in Table 4 together with comparative literature data for related {2Fe2S}-systems. All of the primary processes of the {2Fe3S}-complexes are irreversible or at best partially reversible at room-temperature and moderate scan-rates (< 200 mV s^{-1}) and give rise to a diverse following chemistry. This includes formation of bridging carbonyl, mixed-valence, hydrido and catalytically active intermediates. Detailed mechanistic aspects of these, as probed by a range of electrochemical and spectroelectrochemical methods will be descibed in detail in a subsequent paper; here we confine ourselves to a discussion of trends in potentials, noting that E_p values are indicative rather than thermodynamic measures of relative redox orbital energies.

The general effect of successive substitution of CO for CN^- is that E_p^{ox} and E_p^{red} are shifted to more negative values by around 400–500 mV for both {2Fe2S}- and {2Fe3S}-assemblies as illustrated by Fig. 10 and evident from the Table 4 (compare entries 2,8; 3,6; and 4,7). This is most likely a predominantly electrostatic effect which shifts the HOMO–LUMO redox manifold in tandem as the negative charge density on the complex is increased, Fig. 10. Substitution of CO by CN^- at closed-shell mononuclear centres usually invokes a shift of around 1000 mV, as quantified by the ligand parameter P_L, which is 0.0 and 1.00 V for CO and CN^- respectively.[33] This smaller shift in the binuclear systems is consistent with delocalisation of charge over the two iron centres and this is supported by the general shift in all the FTIR terminal carbonyl frequencies to lower values upon substitution of CO by CN^-.

Formally replacing neutral CO by a neutral pendant thioether ligand leads to a relatively small negative shift in E_p^{red} of less than 100 mV but a considerable negative shift in E_p^{ox} of nearly 500 mV, Table 4 and Fig. 10. Thus the LUMO, which is almost certainly an Fe–Fe anti-bonding (σ*) orbital,[34] can have little CO or thioether ligand character. In contrast, replacing the strong π-acid CO by the thioether ligand significantly perturbs the HOMO which is evidently very sensitive to the Fe

‡ 0.2 mm s^{-1} was subtracted from the i.s. recorded at 4.2 K to compare with the 77 K values reported in this work.[40]

atom environment. That the methyl or benzyl thioether ligand acts as a moderately good donor ligand as indicated by FTIR data discussed above is reinforced by comparison of the E_p^{ox} potentials for **5a**,**b** with $[Fe_2(SC_3H_6S)(CN)(CO)_4(PMe_3)]^-$,[16] Table 4 (entries 6, 7 and 9).

Conclusions

In summary, we have described:

(i) the synthesis of tripodal dithiolate thioether ligands which provide a route to {2Fe3S}-species,

(ii) the X-ray crystallographic structures of carbonyl and carbonyl cyanide species exemplifying the {2Fe3S}-framework,

(iii) fluctionality involving inversion at the thioether sulfur ligand,

(iv) the formation of an intermediate possessing a {2Fe3S}-core, a bridging carbonyl group and differentiated iron atoms each ligated by a cyanide ligand, these structural elements closely relate to those of the di-iron sub-site of hydrogenase,

(v) Mössbauer data which show differentiated iron-sites in the di-iron systems and which provide i.s. and q.s. parameters pertinent to the H-cluster of all-iron hydrogenase.

Bridging/terminal carbonyl interconversions evidently take place during turnover of the hydrogenase system with accompanying making or breaking of the metal–metal bond.[5,25] Here we note that bridging carbonyl formation may provide a means of exposing an enzymic site at which the substrate binds (water/proton) whereas reformation of a metal–metal bond, with CO switching into a terminally bonded mode may provide the mechanism for desorbing the product (dihydrogen). The rearrangement of the bridging carbonyl intermediate **6a** to the Fe–Fe bonded terminal CO isomer **7a**, Scheme 2,[25] has some analogy with the latter possibility. Thus the necessity of a *binuclear centre* in the natural system can be explained by the need to support terminal/bridging CO interconversions.

Experimental

General

All experiments, including ligand synthesis, were carried out under inert atmosphere of nitrogen. Solvents were dried using standard procedures and distilled under nitrogen atmosphere. $[Fe_3(CO)_{12}]$ was purchased from Alfa Aesar, all other reagents were purchased from Aldrich. 1,1,1-Tris(mercaptomethyl)-ethane was prepared according to the literature method.[27] Microanalysis: Microanalysis Service, University of East Anglia, Norwich. NMR: JEOL Lambda 400 MHz. FTIR: Bio-Rad FTS-7 spectrometer equipped with a sealed cell for liquid analysis. Mass spectrometry: School of CPES, University of Sussex. Metal analysis: samples were prepared by dissolving metal complex in HNO_3 and water, samples of known concentration were sent for analysis to Southern Water, Sussex Laboratory, Brighton.

Mössbauer

Spectra were recorded on an ES-Technology MS-105 spectrometer with a 200 MBq ^{57}Co source in a rhodium matrix at ambient temperature. Spectra were referenced to a 25 μm iron foil at 298 K. Parameters were obtained by fitting the data with Lorentzian lines.

Electrochemistry

A two-compartment cell fitted with a vitreous carbon disc working electrode, a platinum wire secondary electrode and either an SCE or Ag wire/ferrocene internal standard reference system was employed for cyclic voltammetric measurements. Experiments were carried out using a Hi-Tek DT 2101 potentiostat interfaced with a Hi-Tek PPR1 waveform generator and data were recorded on a Philips PM 8041 X–Y recorder. The supporting electrolyte $[NBu_4][BF_4]$ (0.1 M in MeCN and 0.2 M in CH_2Cl_2) was prepared following a standard laboratory procedure.

Crystal structure analyses

The analysis of $[Fe_2\{MeSCH_2C(Me)(CH_2S)_2\}(CO)_5]$, complex **4a**, is described here. The analyses of the other samples followed very similar procedures. Crystal data for the three complexes are listed in Table S1 (ESI).†

Crystals are deep red, irregular fragments of diamond-shaped plates. One, *ca.* 0.29 × 0.17 × 0.14 mm, was sealed in a capillary. After preliminary photographic examination, this was transferred to an Enraf-Nonius CAD4 diffractometer (with monochromated radiation) for determination, at room temperature, of accurate cell parameters (from the settings of 25 reflections, θ = 10–11°, each centred in four orientations) and for measurement of diffraction intensities (3528 unique reflections to θ_{max} = 21°, the limit of measurable intensities; of these, 2614 were 'observed' with $I > 2\sigma_I$).

During processing, corrections were applied for Lorentz-polarisation effects, a small deterioration correction, absorption (by semi-empirical ψ-scan methods) and to eliminate negative net intensities (by Bayesian statistical methods). The structure was determined by the direct methods routines in the SHELXS program[36] and refined by full-matrix least-squares methods, on F^2, in SHELXL.[37] There are two essentially identical, independent molecules in the crystal. In one molecule, one of the carbonyl oxygen atoms is disordered over two distinct sites. Hydrogen atoms were included in idealised positions, and the methyl groups were allowed to rotate about the C–C bonds. The non-hydrogen atoms were refined with anisotropic thermal parameters and the H-atom U_{iso} values were set to ride on the U_{eq} values of the parent carbon atoms. At the conclusion of the refinement, $wR_2 = 0.061$ and $R_1 = 0.046$,[37] for all 3528 reflections weighted $w = \sigma^{-2}(F_o^2)$; for the 'observed' data only, $R_1 = 0.028$.

In the final difference map, the highest peaks (to *ca.* 0.24 e Å^{-3}) were close to a carbonyl ligand.

Scattering factors for neutral atoms were taken from ref. 38. Computer programs used in this analysis have been noted above or in Table 4 of ref. 39 and were run on a DEC-AlphaStation 200 4/100 in the Biological Chemistry Department, John Innes Centre.

Complex **5a** was unstable at room temperature and the intensity data were recorded at 140 K.

CCDC reference numbers 195090–195092.

See http://www.rsc.org/suppdata/dt/b2/b209690k/ for crystallographic data in CIF or other electronic format.

Syntheses

$MeC(CH_2S)_2CH_2SH$, (4-methyl-[1,2]dithiolan-4-yl)methanethiol, 2. $(CH_3)_2S_2$ (2.51 mL, 28 mmol) was added to 1,1,1-tris(mercaptomethyl)ethane[27] (4.7 g, 28 mmol) in 200 mL freshly distilled methanol under nitrogen atmosphere. Addition of potassium tert-butoxide (31 mg, 0.28 mmol) produced a change from colourless to yellow after 5 min. The mixture was stirred for an hour and degassed every ten minutes to liberate CH_3SH. Methanol was evaporated and the crude material was distilled to give a yellow oil (2.8 g, 60%), bp 150–152 °C (0.7 mm). Microanalysis: $C_5H_{10}S_3$, found (calc): C, 36.48 (36.12); H, 6.14 (6.06); S, 57.6 (57.9)%. ^1H NMR (400 MHz, $C_6D_5CD_3$): δ 0.73 (3H, s, CH_3), 0.89 (1H, t, ^3J 9 Hz, SH), 2.07 (2H, d, ^3J 9 Hz, CH_2SH), 2.27 [2H, d, ^2J 11.2 Hz, (C*H*HSSC*H*H)], 2.48 [2H, d, ^2J 11.2 Hz, (CH*H*SSCH*H*)]. FTIR (KBr): ν(SH) 2551(m, br) cm^{-1}. EI-MS: *m*/*z* 166 $\{M\}^+$, 133 $\{M - SH\}^+$, 119 $\{M - CH_2SH\}^+$.

$MeC(CH_2SH)_2CH_2SMe$, 2-methyl-2-methylsulfanylmethylpropane-1,3-dithiol, 3a. $MeC(CH_2S)_2CH_2SH$, **2** (5.06 g, 30 mmol), was dissolved in 200 mL freshly distilled THF under

nitrogen atmosphere. NaH (1.26 g of 60% suspension, 31 mmol) was cautiously added over 30 min. After 20 min the mixture turned white, foaming gently. MeI (1.87 mL, 30 mmol) was added and the mixture turned back to yellow. This was stirred for an hour. THF was removed and the residue was quenched by 50 mL NH_4Cl saturated water. 300 mL ether was added and this was washed 3 times with 300 mL water. The organic extract was dried ($MgSO_4$) and the solvent removed under vacuum to give a yellow oil. ^{1}H NMR (400 MHz, $C_6D_5CD_3$): δ 0.90 (3H, s, CCH_3), 1.70 (3H, s, SCH_3), 2.22 (2H, s, CH_2SCH_3), 2.38 [2H, d, ^2J 11.5 Hz, ($CHHSSCHH$)], 2.65 [2H, d, ^2J 11.5 Hz, ($CHHSSCHH$)].

$LiAlH_4$ (2.05 g, 54 mmol) was dissolved in 200 mL distilled ether under nitrogen atmosphere. $MeC(CH_2S)_2CH_2SMe$ (4.95 g, 27 mmol) was added slowly at such rate that moderate reflux occurred. After 15 h at room temperature, the mixture was cooled at 0 °C. 60 mL degassed water was carefully added as the mixture foamed a lot, and this was followed by 100 mL degassed H_2SO_4 (10% solution). The ether layer was washed 3 times with 200 mL degassed water. The organic extract was dried ($MgSO_4$) and the solvent removed under reduced pressure. The crude material was distilled to give $MeC(CH_2SH)_2CH_2SMe$ as a colourless oil (2.7 g, 55%), bp 160 °C (0.7 mm). Microanalysis: $C_6H_{14}S_3$, found (calc): C, 39.26 (39.56); H, 7.70 (7.59); S, 53.0 (52.8)%. ^{1}H NMR (400 MHz, CD_2Cl_2): δ 1.03 (3H, s, CH_3), 1.32 (2H, t, ^3J 9 Hz, SH), 2.13 (3H, s, SCH_3), 2.63 (2H, s, CH_2SCH_3), 2.63 [4H, d, ^3J 9 Hz, ($HSCH_2CCH_2SH$)]. EI-MS: *m*/*z* 182 $\{M\}^+$, 61 $\{CH_2SCH_3\}^+$.

$MeC(CH_2SH)_2CH_2SCH_2Ph$, 2-methyl-2-methylsulfanylbenzylpropane-1,3-dithiol, 3b. $MeC(CH_2S)_2CH_2SH$, **2** (1.40 g, 8.4 mmol), was dissolved in 200 mL freshly distilled THF under nitrogen atmosphere. NaH (0.354 g of 60% suspension, 8.8 mmol) was cautiously added over 30 min. After 20 min the mixture turned white, foaming gently. $PhCH_2Br$ (1.44 mg, 8.4 mmol) was added and the mixture remained cloudy. This was stirred for 30 min. THF was removed and the residue was quenched by 50 mL NH_4Cl saturated water. 300 mL ether was added and this was washed 3 times with 300 mL water. The organic extract was dried ($MgSO_4$) and the solvent removed under vacuum to give a brown–yellow oil. ^{1}H NMR (400 MHz, $CDCl_3$): δ 1.25 (3H, s, CCH_3), 2.68 (2H, s, CH_2SCH_2Ph), 2.88 [2H, d, ^2J 11.3 Hz, ($CHHSSCHH$)], 3.05 [2H, d, ^2J 11.3 Hz, ($CHHSSCHH$)], 3.75 (2H, s, SCH_2Ph), 7.30 (5H, m, $SCH_2C_6H_5$),

$LiAlH_4$ (0.60 g, 15.8 mmol) was dissolved in 200 mL distilled ether under nitrogen atmosphere. $MeC(CH_2S)_2CH_2SCH_2Ph$ (2.2 g, 7.9 mmol) was added slowly at such rate that moderate reflux occurred. After 15 h at room temperature, the mixture was cooled at 0 °C. 60 mL degassed water was carefully added as the mixture foamed a lot, and this was followed by 100 mL degassed H_2SO_4 (10% solution). The ether layer was washed 3 times with 200 mL degassed water. The organic extract was dried ($MgSO_4$) and the solvent removed under reduced pressure. The crude material was distilled to give $MeC(CH_2SH)_2CH_2SCH_2Ph$ as a colourless oil (0.67 g, 31%), bp 105 °C (0.002 mm). ^{1}H NMR (400 MHz, CD_2Cl_2): δ 0.90 (3H, s, CH_3), 1.11 (2H, t, ^3J 9 Hz, SH), 2.46 (2H, s, CH_2SCH_2Ph), 2.47 [4H, d, ^2J 9 Hz, ($HSCH_2CCH_2SH$)], 3.63 (2H, s, SCH_2Ph), 7.24 (5H, m, $SCH_2C_6H_5$). EI-MS: *m*/*z* 258 $\{M\}^+$.

$[Fe_2\{MeSCH_2C(Me)(CH_2S)_2\}(CO)_5]$, 4a. $[Fe_3CO_{12}]$ (1.63 g, 3.2 mmol) was dissolved in 70 mL freshly distilled toluene under nitrogen atmosphere. $MeC(CH_2SH)_2CH_2SMe$ (0.58 g, 3.2 mmol) was added to the mixture and this was stirred at 80 °C for 1 h 30 min. The brown–red solution was allowed to cool to room temperature and was filtered through silica gel (70–230 mesh). A dark brown–red fraction was collected by elution with more toluene, leaving a red material on top of column. Solvent was removed under vacuum and replaced by 20 mL MeCN. Acetonitrile was in turn evaporated down, leaving a brown–red powder (0.67 g, 49%). Single crystals were obtained by dissolving this powder in 50 mL hexane and leaving the solution in the fridge for two days. Microanalysis: $C_{11}H_{12}O_5S_3Fe_2$(0.1hexane) found (calc): C, 31.60 (31.59); H, 3.17 (3.05); S, 18.41 (21.83)%. ^{1}H NMR (400 MHz, CD_2Cl_2): δ 0.90 (3H, s, CH_3), 1.65 [2H, d, ^2J 14 Hz, 2($CCHHS$)], 2.05 (2H, br, CH_2SCH_3), 2.23 [2H, d, ^2J 14 Hz, 2($CCHHS$)], 2.64 (3H, s, SCH_3). FTIR (in CH_3CN): ν(CO) 1925w, 1979(s, br) and 2046m cm^{-1}. EI-MS: *m*/*z* 432 $\{M\}^+$, 404$\{M - CO\}^+$, 376$\{M - 2CO\}^+$, 348$\{M - 3CO\}^+$, 320$\{M - 4CO\}^+$, 292$\{M - 5CO\}^+$, 180$\{MeC(CH_2S)_2CH_2SMe\}^+$, 176$\{Fe_2S_2\}^+$.

$[Fe_2\{PhCH_2SCH_2C(Me)(CH_2S)_2\}(CO)_5]$, 4b. $[Fe_3CO_{12}]$ (0.95 g, 1.9 mmol) was dissolved in 70 mL freshly distilled toluene under nitrogen atmosphere. $MeC(CH_2SH)_2CH_2SCH_2Ph$ (0.49 g, 1.9 mmol) was added to the mixture and this was stirred at 90 °C for 1 h 30 min. The brown–red solution was allowed to cool to room temperature and was filtered through silica gel (70–230 mesh). A dark brown–red fraction was collected by elution with more toluene. Solvent was removed under vacuum, leaving a brown–red powder (0.7 g, 73%). The powder was dissolved in 20 mL MeCN and slow evaporation of the solvent under a stream N_2 led to the deposition of crystalline material. Microanalysis: $C_{19}H_{16}O_5S_3Fe_2$, found (calc): C, 40.26 (40.16); H, 3.57 (3.15); S, 15.9 (18.9)%. ^{1}H NMR (400 MHz, CD_2Cl_2): δ 0.90 (3H, s, CH_3), 1.70 [2H, d, ^2J 14 Hz, 2($CCHHS$)], 1.82 (2H, s, CH_2SCH_2Ph), 2.28 [2H, d, ^2J 14 Hz, 2($CCHHS$)], 4.12 (2H, s, SCH_2Ph), 7.40 (5H, m, $SCH_2C_6H_5$). FTIR (in CH_3CN): ν(CO) 1925w, 1981(s, br), 2046m cm^{-1}. EI-MS: *m*/*z* 508 $\{M\}^+$, 480$\{M - CO\}^+$, 452$\{M - 2CO\}^+$, 424$\{M - 3CO\}^+$, 396$\{M - 4CO\}^+$, 368$\{M - 5CO\}^+$, 267$\{Fe_2SSCH_2Ph\}^+$, 231$\{Fe_2SCH_2C(Me)CH_2S\}^+$, 176$\{Fe_2S_2\}^+$.

$[Et_4N][Fe_2\{MeSCH_2C(Me)(CH_2S)_2\}(CN)(CO)_4]$, 5a. $[Fe_2\{MeSCH_2C(Me)(CH_2S)_2(CO)_5]$ (26 mg, 0.06 mmol) was dissolved in 2 mL freshly distilled acetonitrile. $[Et_4N]CN$ (37 mg, 0.24 mmol) was dissolved in 2 mL MeCN from which 500 μL (0.06 mmol) were syringed and added to the brown–red solution containing the complex. The mixture turned immediately to bright red before returning slowly to brown–red. After 1 h 30 min examination by solution FTIR showed essentially quantitative conversion to **5a**. The solvent was removed under vacuum and the resulting oil was triturated with 5 mL of diethyl ether to give a brown powder which was removed by fitration and dried *in vacuo*. Single crystals suitable for X-ray analysis were obtained by slow diffusion of diethyl ether into an MeCN solution at 4 °C over 1 month. Microanalysis: $C_{19}H_{32}N_2O_4S_3Fe_2.H_2O$, found (calc): C, 39.60 (39.44); H, 5.93 (5.88); N, 4.52 (4.84)%. FTIR (in CH_3CN): ν(CO) 1904s, 1940s, 1978s and ν(CN) 2085m cm^{-1}. FAB-MS: *m*/*z*, 413 $\{[Et_4N][Fe_2S(CNH)(CO)_4]\}^+$.

$[Et_4N][Fe_2\{PhCH_2SCH_2C(Me)(CH_2S)_2\}(CN)(CO)_4]$, 5b. $[Fe_2\{PhCH_2SCH_2C(Me)(CH_2S)_2(CO)_5]$ (60 mg, 0.12 mmol) was dissolved in 4 mL freshly distilled acetonitrile. $[Et_4N]CN$ (55 mg, 0.35 mmol) was dissolved in 1 mL MeCN from which 330 μL (0.12 mmol CN^-) were syringed and added to the brown–red solution containing the complex. The mixture turned immediately to bright red before returning slowly to brown–red. After 1 h 30 min examination by solution FTIR showed essentially quantitative conversion to **5b**. The solvent was removed under vacuum and the resulting oil was triturated with 5 mL of diethyl ether to give a brown powder which was removed by fitration and dried *in vacuo*. Microanalysis: $C_{25}H_{36}N_2O_4S_3Fe_2{\cdot}H_2O$, found (calc): C, 46.03 (45.84); H, 5.84 (5.85); N, 4.40 (4.27); S, 14.86 (14.66)%. FTIR (in CH_3CN): ν(CO) 1904s, 1940s, 1978s and ν(CN) 2084m cm^{-1}. ESI-MS: *m*/*z* 499 $\{M–4CO–CN\}^-$.

Generation of $[Et_4N]_2[Fe_2(\mu\text{-}CO)\{MeSCH_2C(Me)(CH_2S)_2\}(CN)_2(CO)_3]$, 6a. $[Fe_2\{MeSCH_2C(Me)(CH_2S)_2(CO)_5]$ (33 mg, 0.07 mmol) was dissolved in 3 mL freshly distilled acetonitrile. $[Et_4N]CN$ (30 mg, 0.19 mmol) was added to the brown–red solution and the mixture turned immediately to bright red before returning slowly to brown–red. After 50 min at room temperature, the mixture was transferred to a freezer at −10 °C. After 12 days in the freezer, the mixture had turned red and was shown by infrared to be the thermally unstable CO-bridged intermediate. FTIR (in CH_3CN): ν(μ-CO) 1780(m, br), ν(CO) 1879s, 1919s, 1958s, ν(CN) 2074m and 2084m cm^{-1}.

$[K(18\text{-crown-}6)]_2[Fe_2\{MeSCH_2C(Me)(CH_2S)_2\}(CN)_2(CO)_4]$, 7a. $[Fe_2\{MeSCH_2C(Me)(CH_2S)_2(CO)_5]$ (22 mg, 0.05 mmol) was dissolved in 4 mL freshly distilled acetonitrile. A [K(18-crown-6)]CN solution was prepared by dissolving KCN (75 mg, 1.15 mmol) and 18-crown-6 ether (0.30g, 1.15 mmol) in 3 mL MeCN from which 295 μL (0.11 mmol CN^-) were syringed and added to the brown–red solution containing the complex. It was stirred at room temperature for 17 h during which time the mixture gradually turned to bright red. FTIR spectroscopy of the solution showed stoichiometric conversion to the dianion. Solvent evaporation and 4 successive washing steps with diethyl ether led to the isolation of a red solid. FTIR (in CH_3CN): ν(CO) 1870(sh), 1884s, 1922s, 1963s, ν(CN) 2075m cm^{-1}. FAB-MS: *m*/*z*, 413 $\{[K(18\text{-crown-}6)][Fe_2\{MeSCH_2C(Me)(CH_2S)_2(CN)_2(CO)_4]\}^+$, 648 $\{[K(18\text{-crown-}6)][Fe_2\{MeSCH_2C(Me)(CH_2S)_2(CNH)(CN)]\}^+$. Iron analysis, found (calc): 23.0 (23.4) mg L^{-1}. The tetraethyl ammonium salt was prepared in a similar fashion using $[Et_4N]CN$. Microanalysis: $C_{28}H_{52}N_4O_4S_3Fe_2{\cdot}CH_3CN$, found (calc): C, 47.91 (47.51); H, 7.41 (7.26); N, 8.77 (9.23)%.

$[Et_4N]_2[Fe_2\{PhCH_2SCH_2C(Me)(CH_2S)_2\}(CN)_2(CO)_4]$, 7b. $[Fe_2\{PhCH_2SCH_2C(Me)(CH_2S)_2(CO)_5]$ (48 mg, 0.94 mmol) was dissolved in 4 mL freshly distilled acetonitrile. $[Et_4N]CN$ (94 mg, 0.60 mmol) was dissolved in 1 mL MeCN from which 340 μL (0.20 mmol CN^-) were syringed and added to the brown–red solution containing the complex. It was stirred at room temperature for 17 h while the mixture gradually turned to bright red. Solvent was evaporated and solid was obtained by washing the oily product 4 times with CH_2Cl_2 and drying under vacuum for 4 h. Microanalysis: $C_{34}H_{56}N_4O_4S_3Fe_2{\cdot}CH_2Cl_2$, found (calc): C, 47.84 (47.86); H, 6.88 (6.61); N, 6.11 (6.38)%. FTIR (in CH_3CN): ν(CO) 1870(sh), 1984s, 1922s, 1963s, ν(CN) 2075m cm^{-1}. ESI-MS: *m*/*z* 534 $\{M - 2(Et_4N^+) + 2(H^+)\}^-$, 506 $\{M - (2Et_4N^+) + (2H^+) - CO\}^-$, 450 $\{M - (2Et_4N^+) - 2CO - CN\}^-$, 394 $\{M - (2Et_4N^+) - 4CO - CN\}^-$.

Acknowledgements

We thank the BBSRC and the John Innes Foundation for supporting this work. J. R. Sanders is thanked for helpful discussion.

References

1 Y. Nicolet, C. Piras, P. Legrand, C. E. Hatchikian and J. C. Fontecilla-Camps, *Structure (London)*, 1999, **7**, 13–23.
2 J. W. Peters, W. N. Lanzilotta, B. J. Lemon and L. C. Seefeldt, *Science*, 1998, **282**, 1853–1858.
3 Y. Nicolet, B. J. Lemon, J. C. Fontecilla-Camps and J. W. Peters, *Trends Biochem. Sci.*, 2000, **25**, 138–143.
4 A. J. Pierik, M. Hulstein, W. R. Hagen and S. P. J. Albracht, *Eur. J. Biochem.*, 1998, **258**, 572–578.
5 Y. Nicolet, A. L. de Lacey, X. Vernede, V. M. Fernandez, E. C. Hatchikian and J. C. Fontecilla-Camps, *J. Am. Chem. Soc.*, 2001, **123**, 1596–1601.
6 A. L. De Lacey, C. Stadler, C. Cavazza, E. C. Hatchikian and V. M. Fernandez, *J. Am. Chem. Soc.*, 2000, **122**, 11232–11233.
7 Y. Nicolet and J. C. Fontecilla-Camps, *Actual. Chim.*, 2001, 34–37.
8 Y. Nicolet, C. Cavazza and J. C. Fontecilla-Camps, *J. Inorg. Biochem.*, 2002, **91**, 1–8.
9 Z. J. Chen, B. J. Lemon, S. Huang, D. J. Swartz, J. W. Peters and K. A. Bagley, *Biochemistry*, 2002, **41**, 2036–2043.
10 C. V. Popescu and E. Münck, *J. Am. Chem. Soc.*, 1999, **121**, 7877–7884.
11 A. S. Pereira, P. Tavares, I. Moura, J. J. G. Moura and B. H. Huynh, *J. Am. Chem. Soc.*, 2001, **123**, 2771–2782.
12 E. J. Lyon, I. P. Georgakaki, J. H. Reibenspies and M. Y. Darensbourg, *Angew. Chem., Int. Ed.*, 1999, **38**, 3178–3180.
13 M. Schmidt, S. M. Contakes and T. B. Rauchfuss, *J. Am. Chem. Soc.*, 1999, **121**, 9736–9737.
14 A. Le Cloirec, S. P. Best, S. Borg, S. C. Davies, D. J. Evans, D. L. Hughes and C. J. Pickett, *Chem. Commun.*, 1999, 2285–2286.
15 E. J. Lyon, I. P. Georgakaki, J. H. Reibenspies and M. Y. Darensbourg, *J. Am. Chem. Soc.*, 2001, **123**, 3268–3278.
16 F. Gloaguen, J. D. Lawrence, M. Schmidt, S. R. Wilson and T. B. Rauchfuss, *J. Am. Chem. Soc.*, 2001, **123**, 12518–12527.
17 H. X. Li and T. B. Rauchfuss, *J. Am. Chem. Soc.*, 2002, **124**, 726–727.
18 M. Razavet, S. C. Davies, D. L. Hughes and C. J. Pickett, *Chem. Commun.*, 2001, 847–848.
19 Z. X. Cao and M. B. Hall, *J. Am. Chem. Soc.*, 2001, **123**, 3734–3742.
20 H. J. Fan and M. B. Hall, *J. Am. Chem. Soc.*, 2001, **123**, 3828–3829.
21 M. Bruschi, P. Fantucci and L. De Gioia, *Inorg. Chem.*, 2002, **41**, 1421–1429.
22 Z. P. Liu and P. Hu, *J. Am. Chem. Soc.*, 2002, **124**, 5175–5182.
23 M. Razavet, A. Le Cloirec, S. C. Davies, D. L. Hughes and C. J. Pickett, *J. Chem. Soc., Dalton Trans.*, 2001, 3551–3552.
24 M. Razavet, S. J. Borg, S. J. George, S. P. Best, S. A. Fairhurst and C. J. Pickett, *Chem. Commun.*, 2002, 700–701.
25 S. J. George, Z. Cui, M. Razavet and C. J. Pickett, *Chem.: Eur. J.*, 2002, **8**, 4037–4046.
26 A. Winter, L. Zsolnai and G. Huttner, *Z. Naturforsch., B*, 1982, **37**, 1430–1436.
27 C. Kolomyjec, J. Whelan and B. Bosnich, *Inorg. Chem.*, 1983, **22**, 2343–2345.
28 F. Gloaguen, J. D. Lawrence and T. B. Rauchfuss, *J. Am. Chem. Soc.*, 2001, **123**, 9476–9477.
29 D. M. Hoffman and R. Hoffmann, *Inorg. Chem.*, 1981, **20**, 3543–3555.
30 gNMR, Adept Scientific plc, Letchworth, Herts, UK, ver. 4.1, 1999.
31 J. R. Dilworth, S. Morton, M. O'Connor and J. Silver, *Inorg. Chim. Acta*, 1987, **127**, 91–92.
32 V. V. Matveev, B. I. Kolobkov and A. I. Nekhaev, *Bull. Acad. Sci. USSR Div. Chem. Sci. (Engl. Transl.)*, 1987, **36**, 2431–2433.
33 J. Chatt, C. T. Kan, G. J. Leigh, C. J. Pickett and D. R. Stanley, *J. Chem. Soc., Dalton Trans.*, 1980, 2032.
34 B. K. Teo, M. B. Hall, R. F. Fenske and L. F. Dahl, *Inorg. Chem.*, 1975, **14**, 3103–3117.
35 A. Darchen, H. Mousser and H. Patin, *J. Chem. Soc., Chem. Commun.*, 1988, 968–970.
36 G. M. Sheldrick, *Acta Crystallogr., Sect. A*, 1990, **46**, 467–473.
37 G. M. Sheldrick, SHELXL-Program for crystal structure refinement, University of Göttingen, Germany, 1993.
38 *International Tables for X-ray Crystallography*, Kluwer Academic Publishers, Dordrecht, 1992, vol. C, pp. 500, 219 and 193.
39 S. N. Anderson, R. L. Richards and D. L. Hughes, *J. Chem. Soc., Dalton Trans.*, 1986, 245–252.
40 N. N. Greenwood and T. C. Gibb, *Mössbauer Spectroscopy*, Chapman and Hall Ltd, London, 1971.